Thermoelectric properties of $Co_xNi_{4-x}Sb_{12-y}Sn_y$ ternary skutterudites

Jon A. Mackey[1]
Mechanical Engineering, University of Akron, Akron, Ohio, 44325

Frederick W. Dynys
NASA Glenn Research Center, Cleveland, Ohio, 44135

and

Alp Sehirlioglu
Materials Science and Engineering, Case Western Reserve University, Cleveland, Ohio, 44106

Thermoelectric materials based on the skutterudite crystal structure have demonstrated enhanced performance (ZT>1), along with good thermal stability and favorable mechanical properties. Binary skutterudites, with single and multiple fillers, have been intensively studied in recent years. Compared to binary skutterudites, the ternary systems have received less attention, e.g. $Ni_4Sb_8Sn_4$. Ternary skutterudites are isoelectronic variants of binary skutterudites; cation substitutions appear to be isostructural to their binary analogues. In general, ternary skutterudites exhibit lower thermal conductivity. Ternary systems of $Ni_4Bi_8Ge_4$, $Ni_4Sb_8Ge_4$, and $Ni_4Sb_8Sn_4$ were investigated using combined solidification and sintering steps. Skutterudite formation was not achieved in the $Ni_4Bi_8Ge_4$ and $Ni_4Sb_8Ge_4$ systems; skutterudite formation occurred in $Ni_4Sb_8Sn_4$ system. P-type material was achieved by Co substitution for Ni. Thermoelectric properties were measured from 298 K to 673 K for $Ni_4Sb_8Sn_4$, $Ni_4Sb_7Sn_5$ and $Co_2Ni_2Sb_7Sn_5$. N-type $Ni_4Sb_8Sn_4$ exhibit the highest figure of merit of 0.1 at 523 K.

I. Introduction

Thermoelectric materials have the potential to provide simple and reliable energy conversion of low grade waste heat. A material figure of merit, $ZT = \alpha^2 T/\rho\kappa$, governs the conversion efficiency of thermoelectric devices. The Seebeck coefficient α must be large, and electrical resistivity ρ and the thermal conductivity κ must be small at a temperature T to create an efficient thermoelectric device [1]. To satisfy these material challenges requires semiconducting materials with low thermal conductivity. Additionally, strong thermoelectric materials must exhibit thermal stability.

Skutterudites have proven to be a suitable system with potential for high ZT, thermal stability, and favorable mechanical properties. Skutterudite structure is represented by a chemical formula of MX_3 and body-centered cubic space group *Im*3, where M is Co, Rh, or Ir and X is P, As, or Sb. A prominent feature of the skutterudite structure is the existence of two relatively large voids per unit cell and four member planar pnictogen rings. The cubic unit cell

[1] Mechanical Engineering, Auburn Science and Engineering Center Room 101, University of Akron, Akron, Ohio, 44325 email: jam151@zips.uakron.edu

can then be written in a general formula as $\square_2M_8X_{24}$ [2]. Most binary skutterudite compounds exhibit large Seebeck coefficients and good electrical conductivity, resulting in large power factor values. Filler cations are inserted in the voids to reduce thermal conductivity and improve ZT. Numerous skutterudite compositions have been investigated and characterized over a wide range of temperatures. Common binary skutterudites studied include $CoSb_3$ [3-8], $CoAs_3$ [7,8], and $FeSb_3$ [9,10]. Binary skutterudites have been studied with a number of different filler elements. A variety of fillers are added in an effort to cover large frequency spectra for phonon scattering, thereby reducing lattice thermal conductivity.

Ternary skutterudites may be formed from a binary variant though isovalent replacement on either the anion or cation site. Several ternary skutterudites are possible such as $CoGe_{1.5}S_{1.5}$ [11], $CoGe_{1.5}Se_{1.5}$ [11], $IrGe_{1.5}S_{1.5}$ [12], $IrGe_{1.5}Se_{1.5}$ [12], $IrSn_{1.5}S_{1.5}$ [12], $RhGe_{1.5}S_{1.5}$ [12], and $Co_4Ge_6Se_6$ [13]. A list of theoretically possible binary and ternary skutterudite compounds is listed by the work of Bauer et al. [14]. In this work, three potential skutterudite systems are investigated: $Ni_4Bi_8Ge_4$, $Ni_4Sb_8Ge_4$, and $Ni_4Sb_8Sn_4$. Skutterudite phase has previously been reported for the $Ni_4Sb_8Sn_4$ system, synthesized by a Sn-flux method [15,16]. This work reveals that both n-type and p-type can be achieved in $Ni_4Sb_7Sn_5$ system, p-type achieved by Co substitution for Ni.

II. Experimental

A variety of fabrication techniques were investigated for sample preparation; including solidification, mechanical alloying, sintering, and a combination of them. The specific processing details for each composition will be discussed in the related sections for each material. Alloy ingots were prepared by direct melting of the metal constituents. Solidification was performed in a graphite resistance heated furnace (Thermal Technology LLC, Santa Rosa, CA) under He atmosphere. Temperature was controlled by a combination of thermocouples and optical pyrometer. Samples were contained in fused silica crucibles (Momentive Performance Materials, Albany, NY) which were placed in a threaded graphite container (Graphite Sales Inc, Chagrin Falls, OH) sealed with a grafoil gasket.

Mechanical alloying was performed using PM100 planetary mill (Retsch, Haan, Germany) with a 125 ml tungsten carbide milling jar (Retsch). Milling was performed at a ball to powder weight ratio of 3.8. The planetary milling was performed in an Ar filled glovebox (MBRAUN,Garching, Germany), to minimize oxygen/moisture exposure.

Sintered discs were derived from the milled powders by several techniques:

(i) Pressure assisted sintering: Hot pressing was performed using a custom fabricated system. Powders were pressed in ½" graphite dies. A pressure of 62 MPa was applied to the die at room temperature before evacuating the chamber. The sample was then heated to 100°C and allowed to outgas before introducing Ar atmosphere. Temperature was then increased to 250°C at a rate of 1.5°C/min. After holding at 250°C for ½ hour, the sample was allowed to cool to room temperature at <1.5°C/min. A thermocouple mounted near the outside of the die provided the temperature control. In addition to temperature and pressure control, the ram travel was also monitored.

(ii) Pressure-less sintering: Pressure-less sintering was performed on cold pressed samples. Disc shaped samples were pressed in a ½" stainless steel die at 140 MPa. Specimens were then sintered in a quartz tube furnace under a N_2 atmosphere.

(iii) Microwave (MW) sintering: MW sintering was performed with a 2 kW 2.45 GHz Single Mode Microwave System (Gerling Applied Engineering Inc., Modesto, CA). Discs of ½" diameter were cold pressed in stainless steel dies at 140 MPa and MW sintered under a N_2 atmosphere using a quartz enclosure. The waveguide was configured to obtain a standing wave within the region of the quartz enclosure that holds the sample. An automatic impedance analyzer (Homer, S-Team, Bratislava, Slovak Republic) with a motorized three-stub tuner was used to keep the microwave cavity tuned. An optical pyrometer provided temperature feedback.

X-ray diffraction (XRD) was performed on a D-8 Advance Instrument (Bruker, Billerica, MA) with Cu Kα radiation. Data was collected in a Bragg-Brentano configuration over 10-80° at a rate of 3.5° per minute. Microstructure was investigated with a Hitachi S-4700 scanning electron microscope (SEM) (Hitachi High Technologies, Gaithersburg, MD) equipped with energy dispersive spectroscopy (EDAX, Mahwah, NJ). Operating accelerating voltages ranged from 15 to 20 kV.

Seebeck coefficient and electrical resistivity were measured with a modified ZEM-3 system (ULVAC Technologies, Methuen, MA). The system performs a four-point resistivity measurement, the details of which are discussed in reference 17. Measurements were performed in He atmosphere at 85 Torr, and temperature range of 25-400°C. Test electrical currents were less than 50 mA, and test thermal gradients were less than 1°C/mm. Seebeck and electrical resistivity measurements were preformed on 4x4x18 mm samples; sample measurement direction was parallel to the pressing direction. Thermal diffusivity was measured using the laser flash method (Anter Flashline 5000, TA

Instruments, New Castle, DE). Measurements followed ASTM E1461. Thermal diffusivity was measured from 25-400°C under N_2 atmosphere on disc shaped samples with 3 mm thickness and 12.5 mm diameter. Sample faces were coated with carbon paint to ensure reproducible emissivity. Thermal conductivity was calculated from thermal diffusivity, density, and calculated specific heat. Sample density was measured by the submersion method using methyl ethyl ketone as the fluid. Specific heat was calculated following the rule of mixtures along with the Dulong-Petit law. Specific heat calculations were confirmed using a Pyroceram standard in the laser flash method. The thermal diffusivity measurement was parallel to the pressing direction. Room temperature Hall coefficient was measured on a 7600 Hall effect system (Lake Shore Cryotronics, Westerville, OH). Samples were measured in Van der Pauw configuration with applied field of 2 T and electrical current of 50 mA. Samples were discs cut parallel to the pressing direction with 0.5 mm thickness and 12.5 mm diameter.

III. Processing

A. $Ni_4Bi_8Ge_4$

Initial attempt to synthesize the desired skutterudite phase was solidification. Elemental constituents were melted for 2 hours at 1100°C at heating and cooling rates of +20°C/min and -10°C/min, respectively. Due to the lack of a ternary phase diagram for this system, processing temperatures were based on binary phase diagrams. Crucibles were weighed before and after solidification and material loss was found to be less than 1%. Phase segregation was observed in the ingot (Fig. 1). It consisted of a Bi phase (melting temperature 271°C) surrounding a region of NiGe (peritectic temperature 850°C) and $Ni_{2.74}Ge_2$ phases. Skutterudite phase was not achieved; furthermore Bi did not react with the Ni/Ge components.

In an attempt to react Bi with Ni, a sample was prepared by melting stoichiometric amounts of Ni and Bi for 1 hour at 1150°C (+20°C/min, -10°C/min). The phases in the ingot were identified as Bi, $NiBi_3$ (peritectic temperature 469°C), and NiBi (peritectic temperature 654°C). The ingot was then crushed and combined with stoichiometric amount of Ge and re-melted for 1 hour at 1150°C (+20°C/min, -10°C/min). The final ingot was similar to that shown in figure 1, consisting of a large region of segregated Bi surrounding a region of Ni_xGe phases. The ingot was annealed at 600°C for 67 hours in N_2 atmosphere. Annealing did not change the sample phase content. It was evident from the microstructural analysis that Bi melted and solidified during annealing, while the Ni_xGe phase appeared to remain intact. Thus, Ni_xGe is not highly soluble in liquid Bi.

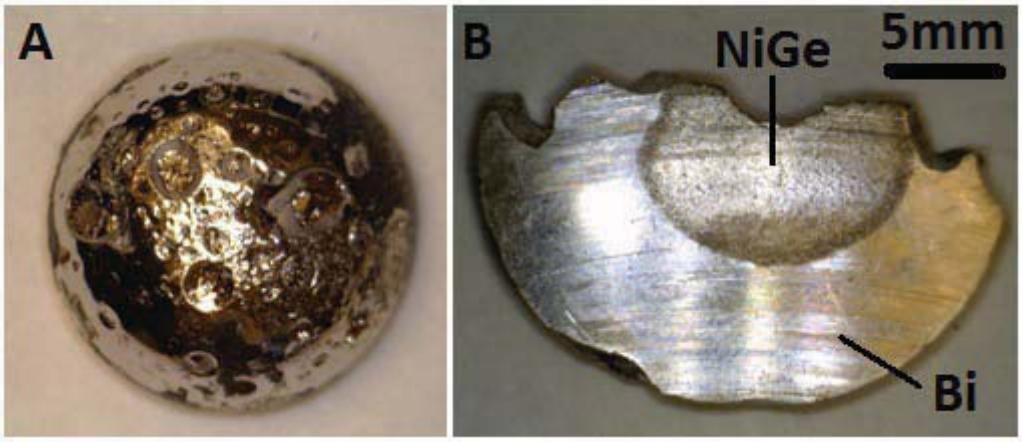

Figure 1: A) Ingot of Ni/Bi/Ge melt (25 mm diameter). B) Cross-section view of ingot showing phase segregation of Bi and Ni_xGe phases.

Powder processing was also pursued. The elemental powders were milled for 7 hours at 580 rpm. Milling consisted of 1 hour intervals; the powder was scraped from the wall of the milling jar between each interval. Densification of powders was performed by MW sintering. Samples were processed at both low power (200 W -4 min) and higher power (~400 W -34 min). Low MW power was chosen to avoid possible melting and segregation of the Bi phase. However, Bi still melted and formed a Bi rich outer layer on portions of the sample. Both the low and high power MW sintered samples exhibited porosity and heterogeneous microstructure of Bi and Ni_xGe phases. Higher density was achieved at the higher MW power, 5.7 g/cc vs. 4.6 g/cc at low power. The microstructure of the specimen sintered at low power MW is shown in figure 2; light phase is Bi whereas the darker phases are Ni_xGe. Additionally, not shown in figure 2, some outer regions consisted exclusively of segregated Bi.

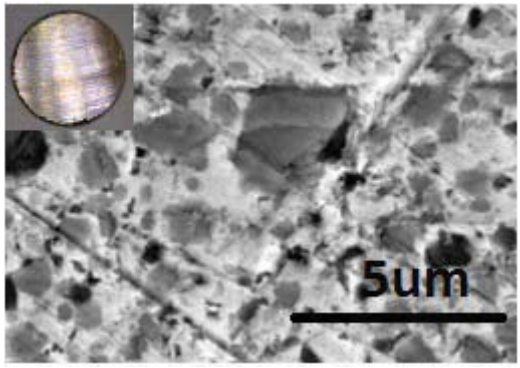

Figure 2: Secondary electron SEM micrograph of microwave sintered sample showing heterogeneous phases and porosity. Inset) cross-section view of sample.

In addition, milled powders were hot pressed, in an attempt to reactively hot press the desired phase. Pellets were densified at 180°C for 30 minutes under an applied pressure of 62 MPa in Ar atmosphere. Higher temperatures

caused formation of liquid phase and catastrophic die failure. Similar to the specimens obtained through solidification, the final pellets were composed of a heterogeneous mixture of Bi and Ni_xGe phases. The electrical resistivity of the Bi and Ni_xGe composites averaged 0.50 mOhm*cm at room temperature and 0.55 mOhm*cm at 250°C. The Seebeck coefficient of the composites averaged -52 μV/K at room temperature and -41 μV/K at 250°C. Thermal conductivity was not measured on the samples. An approximate figure of merit was calculated by using estimated thermal data for the primarily Bi composites. The maximum figure of merit on these Bi/Ni_xGe composites is likely less than 0.06 at a peak temperature of 150°C. More detailed thermoelectric characterization was not performed, as ternary skutterudite could not be achieved for this system.

B. $Ni_4Sb_8Ge_4$

Powder processing route was utilized by milling the elemental constituents. Milling proceeded at 1 hour intervals at 300 rpm for the first 12 hours and 550 rpm for the remaining time (19 hours maximum). Powder was scrapped off the milling jar wall at each interval. Figure 3 shows selected XRD profiles of the mechanically alloyed powder at selected times. After 2 hours of milling, the identified phases were Ni, Sb, and Ge. After 13 hours, NiSb phase formed, and this phase continued to grow in quantity as the milling time increased. The final powder consisted of Sb, Ge, and NiSb phases. Broadening of the reflections throughout the milling study suggested reduction of crystallite domain size.

When pressed discs were pressure-less sintered at 600°C for 35 hours in N_2, liquid phase rich in Sb (melting temperature 630°C) formed and segregated during densification. Decreasing the sintering temperature to 550°C (for 20 hours) resulted in elimination of the liquid phase. Skutterudite phase did not form at either sintering conditions. Phases observed were Sb, $Ni_{2.74}Ge_2$, Ni, and Ge. Figure 4 shows the microstructure; it consisted of a large amount of porosity (black regions) and a heterogeneous mixture of Ni_xGe (dark gray) and Sb (light) phases. A similar microstructure was observed for the Ni/Bi/Ge system.

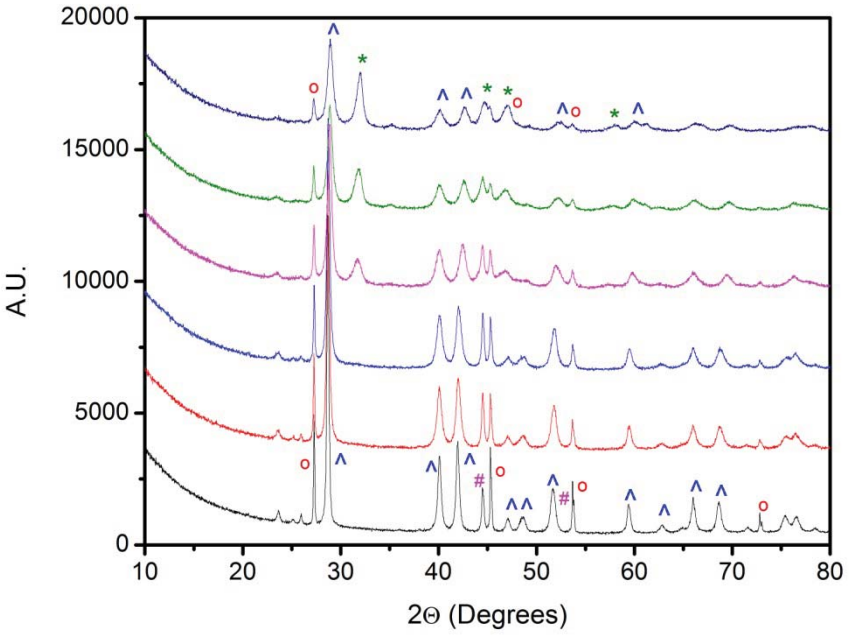

Figure 3: XRD of milling study on Ni/Sb/Ge system, milling interval between selected profiles was 1-3 hours. Bottom profile (milling time 2 hours) contains Sb (^), Ge (o), and Ni (#) phases. Top profile (milling time 19 hours) contains Sb (^), NiSb (*), and Ge (o) phases.

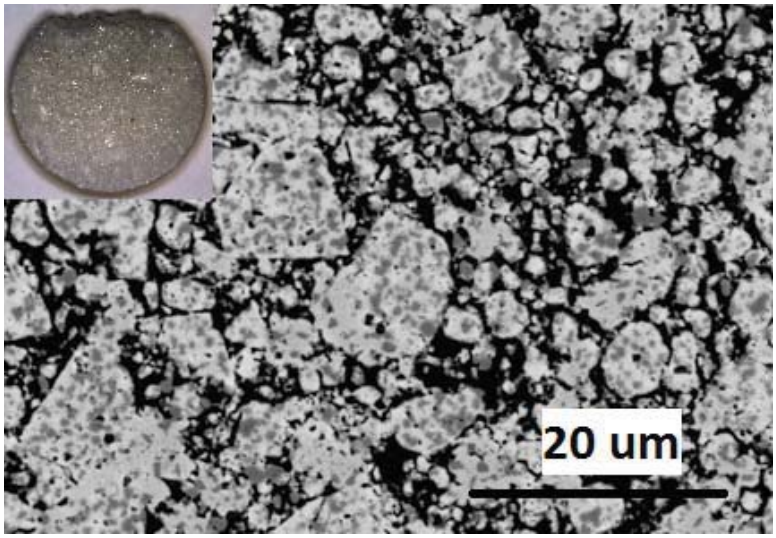

Figure 4: Backscattered SEM micrograph of cold pressed and sintered sample showing heterogeneous phases and porosity. Inset) cross-section view of sample.

C. $Ni_4Sb_8Sn_4$

Skutterudite phase was achieved by using a multistep process by combining several of the aforementioned techniques. Elemental constituents of the Ni/Sb/Sn system were melted for 2 hours at 1100°C, (+20°C/min, -10°C/min). The ingot phases were SbSn (melting temperature 330°C), NiSb (melting temperature 1147°C), and $NiSb_2$ phases (melting temperature 621°C). The morphology of the ingot was not homogenous. The top portion of the ingot was porous and exhibited dendritic microstructure; whereas the lower portion was fully dense. To ensure a clean sample, the top 3 mm of the ingot was discarded and the remainder of the ingot was crushed into a powder. The second process step was milling the crushed powder at 580 rpm with 1 hour intervals. Between each interval powder was scrapped from the wall of the jar. The XRD profiles of the milling study (Fig. 5) show the initial formation of the desired $Ni_4Sb_8Sn_4$ skutterudite phase after 4 hours. As the milling time increased, the relative intensity of the XRD reflections of the skutterudite phase grew and secondary phases decreased. The final skutterudite phase, exhibit a lattice parameter 0.91 nm and lorentzian crystallite domain size of 51 nm. The final milled powder had the following phase composition: 97 wt% skutterudite phase, 1.8 wt% NiSb and the remaining 1.2 wt.% being SbSn and $NiSb_2$ phases. Phase properties were determined by Rietveld refinement on the XRD data from 10 to 80°. Data was obtained with a Bragg-Brentano configuration with 250 mm radius, 4° soller slits, at a rate of 3.5° per minute. The model had an Rexp value of 2.81 and a GOF 1.38.

Direct milling of the elemental constituents (Ni/Sb/Sn) did not produce the skutterudite phase. The starting elements were too ductile, unlike the phases achieved from the solidified ingot which mill into fine powder without agglomerating.

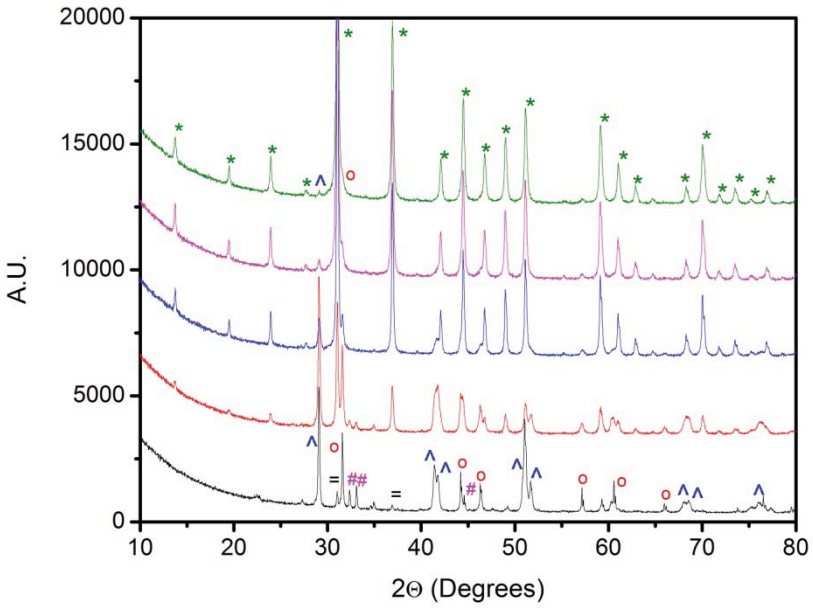

Figure 5: XRD of milling study on Ni/Sb/Sn system, milling interval between profiles was 3 hours. Bottom profile (milling time 1 hour) contains SbSn (^), NiSb (o), $NiSb_2$ (#), $NiSn_{0.75}$ (=), and Ni phases. Top profile (milling time 13 hours) contains $Ni_4Sb_8Sn_5$ (*) phase with trace amounts of SbSn (^) and NiSb (o).

The third process step was hot pressing the milled ingot powder at 250°C for 30 minutes at 62 MPa in Ar atmosphere. The fabricated samples exhibited densities >99% (theoretical 7.34 gcc) . The microstructure (Fig. 6) consisted of a $Ni_4Sb_8Sn_4$ skutterudite matrix with SbSn precipitates on the order of 1 μm. XRD of crushed sample contained 98 wt% skutterudite phase with the remaining phases being SbSn and NiSb.

In addition to hot pressing, lower sintered densities were achieved by pressure-less sintering. Cold pressed pellets were sintered under an N_2 atmosphere at 500°C for 16 hours. Resulting porosity was greater than 26%. Skutterudite phase content was 88.7 wt%, with remaining constituents being 9.6 wt% SbSn and 1.6 wt% NiSb. XRD phase quantification was determined by Rietveld refinement, with GOF 3.02. Figure 7 shows an optical image of the pellet. The dark phase is porosity, which is in agreement with the low measured density; the inset shows the sintered pellet.

Using multi-step processing two more skutterudite compositions were successfully fabricated by increasing Sn concentration, $Ni_4Sb_7Sn_5$ and $Co_2Ni_2Sb_7Sn_5$.

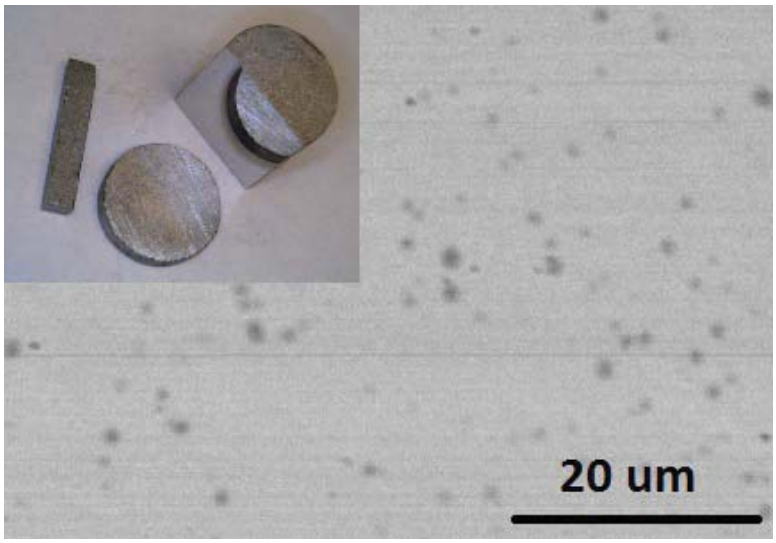

Figure 6: Backscattered SEM micrograph of hot pressed $Ni_4Sb_8Sn_4$ sample showing skutterudite matrix with SbSn precipitates. Inset) hot pressed sample along with samples for thermoelectric characterization.

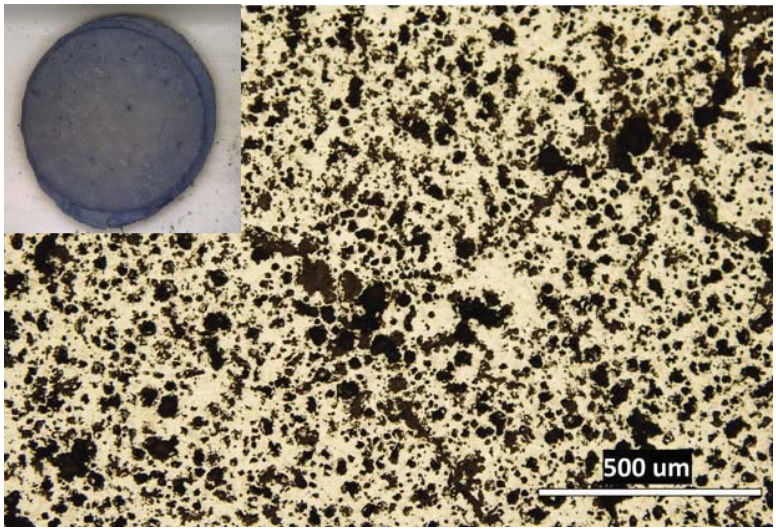

Figure 7: Optical micrograph of $Ni_4Sb_8Sn_4$ sample prepared from cold pressing and sintering, displaying 26% porosity. Inset) sintered pellet.

IV. Thermoelectric Properties

The systems investigated exhibited both n-type ($Ni_4Sb_8Sn_4$ and $Ni_4Sb_7Sn_5$) and p-type ($Co_2Ni_2Sb_7Sn_5$) behavior. Tuning of the carrier type was achieved by substitution of Co for Ni on the Wyckoff 8c position. Standard valence electron counting (VEC) predicts n and p-type semiconducting behavior [18]. For $Ni_4Sb_8Sn_4$, a simple bonding scheme suggested 10 valence electrons from each Ni transition metal with 3 valence electrons for the Sb pnictogen atoms and 2 valence electrons for the Sn substitution atoms, giving a total VEC of 72. As in the case of typical

highly doped semiconductors, the electrical resistivity and Seebeck data (Fig. 8) suggested an extrinsic conduction region with increasing resistivity and Seebeck coefficient and a high temperature intrinsic region. At high temperatures both the resistivity and Seebeck coefficient decreased with increase in temperature, likely due to thermally excited bipolar conductors. The system exhibits low Seebeck coefficients, less than 60 μV/K, consistent with the high carrier densities measured $\geq 2x10^{21}$ cm^{-3}. Electrical resistivity of the n-type samples ranged from 225-275 μOhm-cm while the p-type sample ranged from 290-440 μOhm-cm. The carrier density needs to be further decreased to $2x10^{19}$ cm^{-3} range to optimize electronic properties for thermoelectric applications. The electrical data for $Co_2Ni_2Sb_7Sn_5$ showed a sharp discontinuity around 250°C (figure 8, seen in both resistivity and Seebeck). This discontinuity corresponded to a phase change observed in differential thermal analysis; melting of Ni_3Sn_4 one of the secondary phases in the system. While all of the samples contained small amounts of secondary phases, this secondary phase with low melting temperature was found only in the Co containing sample.

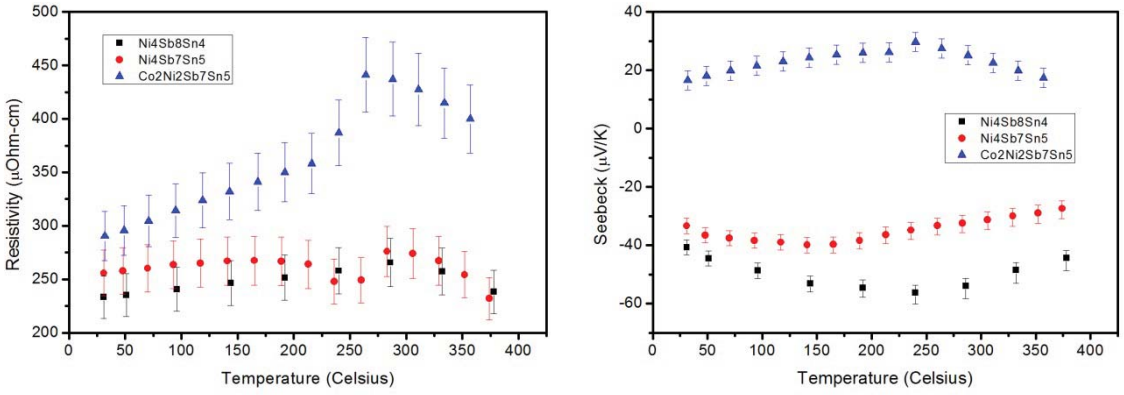

Figure 8: Left) Electrical resistivity of ternary skutterudite phase versus temperature. Right) Seebeck coefficient of ternary skutterudite phase versus temperature.

Thermal conductivity is shown in figure 9. Lattice component of the thermal conductivity was calculated using the Wiedemann-Franz law employing the classic Lorentz number (2.44E-8 W Ohm K^{-2}). The low Seebeck coefficients of the samples justified the use of the classic Lorentz number. Thermal conductivity of the samples ranged from 4-9 W/m-K with lattice component ranging from 0.6-3 W/m-K with temperature. Similar to the electrical data, a sharp property change occurred in the $Co_2Ni_2Sb_7Sn_5$ sample around the melting temperature of the Ni_3Sn_4 phase; approximately 250°C.

The figure of merit for this system was low; maximum ZT was 0.1 (Fig. 9). The high carrier density resulted in low Seebeck coefficients, which caused the low figure of merit. Two optimization paths exist for tuning the system i) electronic improvements through tuning carrier density and ii) lattice conductivity reductions through rattlers and lattice substitution point defects. Using a straight forward single parabolic band model to estimate the potential of the system, a maximum ZT of 0.5 at 127°C was calculated for a carrier density of $2x10^{19}$ cm^{-3}. Additional improvements in ZT could be achieved through addition of fillers on the empty Wyckoff 2a site.

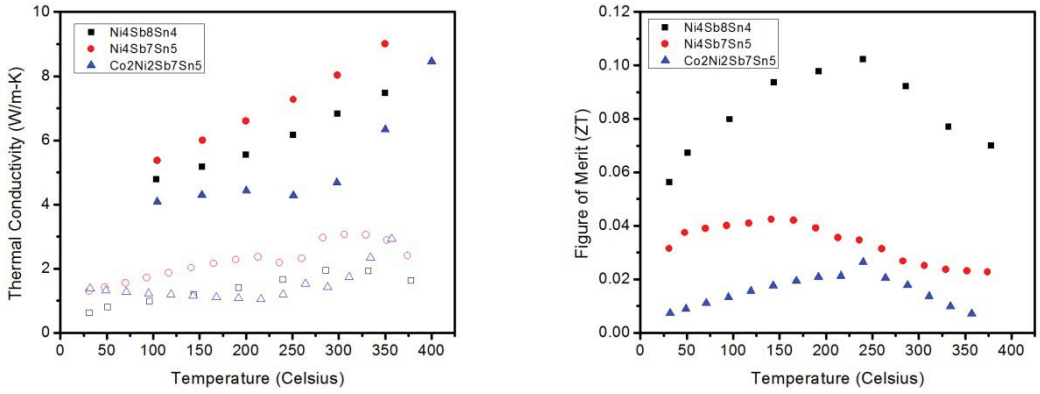

Figure 9: Left) Thermal conductivity versus temperature; closed symbols for total thermal conductivity, open symbols for lattice thermal conductivity. Right) Material figure of merit versus temperature.

V. Conclusion

Ternary skutterudite systems were investigated with a number of processing routes. Formation of a skutterudite phase was not achieved for the $Ni_4Bi_8Ge_4$ and $Ni_4Sb_8Ge_4$ systems. Skutterudite phase occurred for $Ni_4Sb_8Sn_4$, $Ni_4Sb_7Sn_5$ and $Co_2Ni_2Sb_7Sn_5$ compositions. Thermoelectric properties were measured from 25-400°C for the n-type $Ni_4Sb_8Sn_4$ and $Ni_4Sb_7Sn_5$ and p-type $Co_2Ni_2Sb_7Sn_5$ samples. Electrical resistivity ranged from 225-275 μOhm-cm for n-type samples and 290-440 μOhm-cm for the p-type sample. Thermal conductivities ranged from 4-9 W/m-K with lattice components of 0.6-3 W/m-K. Low Seebeck coefficients, <60 μV/K, result in a low figure of merit for the system, with a peak ZT of 0.1 at 250°C. The low Seebeck coefficient of the system is consistent with high measured carrier densities of $>2x10^{21}$ cm^{-3}.

Acknowledgments

The authors would like to thank Ben Kowalski, Tom Sabo, and Ray Babuder from Case Western Reserve University and NASA Glenn Research Center. This work was funded through NASA cooperative agreement NNX08AB43A.

References

1. B. Sherman, R.R. Heikes, and R.W. Ure, Calculation of Efficiency of Thermoelectric Devices, J. Appl. Phys. **31**, 1-17 (1960).

2. K.S. Aleksandrov and B.V. Beznosikov, Crystal Chemistry and Prediction of Compounds with a Structure of Skutterudite Type, Crystallogr. Rep. **52**, 28-36 (2007).

3. A. Grytsiv, P. Rogl, H. Michor, E. Bauer, and G. Giester, InyCo4Sb12 Skutterudite: Phase Equilibria and Crystal Structure, J. Electron. Mater. **42**, 2940-2952 (2013).

4. J. Eilertsen, S. Rouvimov, and M.A. Subramanian, Rattler-seeded InSb nanoincluisons from metastable indium-filled In0.1Co4Sb12 skutterudites for high-performance thermoelectrics, Acta Mater. **60**, 2178-2185 (2012).

5. X. Shi, J. Yang, J.R. Salvador, M. Chi, J.Y. Cho, H. Wang, S. Bai, J. Yang, W. Zhang, and L. Chen, Multiple-Filled Skutterudites: High Thermoelectric Figure of Merit through Separately Optimizing Electrical and Thermal Transports, J. Am. Chem. Soc. **133,** 7837-7846 (2011).

6. D.T. Morelli, G.P. Meisner, B. Chen, S. Hu, and C. Uher, Cerium filling and doping of cobalt triantimonide, Phys. Rev. B. **56**, 7376-7383 (1997).

7. J. Ackerman and A. Wold, The Preparation and Characterization of the Cobalt Skutterudites CoP3, CoAs3, and CoSb3, J. Phys. Chem. Solids **38**, 1013-1016 (1977).

8. G. Kliche and H.D. Lutz, Temperature Dependence of the FIR Reflection Spectra of the Skutterudites CoAs3 and CoSb3, Infrared Phys. **24**, 171-177 (1984).

9. P.F. Qiu, R.H. Liu, J. Yang, X. Shi, X.Y. Huang, W. Zhang, L.D. Chen, J. Yang, and D.J. Singh, Thermoelectric Properties of Ni-doped CeFe4Sb12 Skutterudites, J. Appl. Phys. **111**, 023705 (2012).

10. P.F. Qiu, J. Yang, R.H. Liu, X. Shi, X.Y. Huang, G.J. Snyder, W. Zhang, and L.D. Chen, High-temperature electrical and thermal transport properties of fully filled skutterudites RFe4Sb12 (R=Ca, Sr, Ba, La, Ce, Pr, Nd, Eu, and Yb), J. Appl. Phys. **109**, 063713 (2011).

11. R. Korenstein, S. Soled, A. Wold, and G. Collin, Preparation and Characterization of the Skutterudite-Related Phases CoGe1.5S1.5 and CoGe1.5Se1.5, Inorg. Chem. **16**, 2344-2346 (1977).

12. A. Lyons, R.P. Gruska, C. Case, S.N. Subbarao, and A. Wold, The preparation and characterization of some skutterudite related compounds, Mat. Res. Bul. **13**, 125-128 (1978).

13. Y. Dong, K. Wei, and G.S. Nolas, Transport properties of partially filled skutterudite derivatives Ce0.13Co4Ge6Se6 and Yb0.14Co4Ge6Se6, Phys. Rev. B. **87**, 195203 (2013).

14. E. Bauer, St. Berger, M. Della Mea. G. Hilscher, H. Michor, and Ch. Paul, Filled skutterudites: formation, ground state properties and thermoelectric features, Acta Phys. Pol., B **34**, 595-608 (2003).

15. A. Grytsiv, P. Rogl, St. Berger, Ch. Paul, H. Michor, E. Bauer, G. Hilscher, C. Godart, P. Knoll, M. Musso, W. Lottermoser, A. Saccone, R. Ferro, T. Roisnel, and H. Noel, A novel skutterudite phase in the Ni-Sb-Sn system: phase equilibria and physical properties, J. Phys.: Condens. Matter **14**, 7017-7090 (2002).

16. St. Berger, Ch. Paul, H. Michor, E. Bauer, G. Hilscher, A. Grytsiv, and P. Rogl, Crystal structure and thermoelectric properties of novel skutterudite EpyNi4Sb12-xSnx with Ep=Sn, Eu, and Yb, 21st International Conference on Thermoelectrics **2**, 48-51 (2002).

17. J.Mackey, F. Dynys, and A. Sehirlioglu, Uncertainty analysis for common Seebeck and electrical resistivity measurement systems, Submitted (2014).

18. J.P. Fleurial, T. Cailliat, and A. Borshchevsky, Skutterudites: An Update, 16th International Conference on Thermoelectrics (1997).